ELSEVIER

International Journal of Heat and Fluid Flow 21 (2000) 134–145

International Journal of HEAT AND FLUID FLOW

www.elsevier.com/locate/ijhff

Heat transfer on a film-cooled rotating blade

V.K. Garg *

AYT Corporation, NASA Glenn Research Center, Mail Stop 5-11, Cleveland, OH 44135, USA

Received 29 June 1999; accepted 3 October 1999

Abstract

A multi-block, three-dimensional Navier–Stokes code has been used to compute heat transfer coefficient on the blade, hub and shroud for a rotating high-pressure turbine blade with 172 film-cooling holes in eight rows. Film-cooling effectiveness is also computed on the adiabatic blade. Wilcox's k–ω model is used for modeling the turbulence. Of the eight rows of holes, three are staggered on the shower-head with compound-angled holes. The multi-block grid consists of 4818 elementary blocks which were merged into 280 super blocks. The viscous grid has nearly two million cells. Each hole-exit, in its true oval shape, has 80 cells within it so that coolant velocity, temperature, k and ω distributions can be specified at these hole-exits. For the given parameters, heat transfer coefficient on the cooled, isothermal blade is found to be high in the tip region, and in the leading edge region between the hub and blade mid-span. The effectiveness over the cooled, adiabatic blade is the lowest in these regions. Results for an uncooled blade are also shown, providing a direct comparison with those for the cooled blade. The heat transfer coefficient is much higher on the blade tip and shroud as compared to that on the hub for both the cooled and the uncooled cases. Effect of gridding the tip clearance gap vs. use of a tip clearance model, as well as the effect of different orientation of coolant ejection from shower-head holes is found to be small as far as the heat transfer coefficient or the adiabatic effectiveness on the blade surface is concerned.

Keywords: Film-cooling; Rotating turbine blade; Heat transfer; Adiabatic effectiveness

Notation

B_p	blowing parameter $\{=(\rho_c V_c)/[\rho_{o,in}(RT_{o,in})^{1/2}]\}$
d	coolant hole diameter
h	heat transfer coefficient (in W/m^2 K) based on $(T_{o,rel}-T_w)$
k	turbulence kinetic energy
l	turbulence length scale
m	mass flow rate
m_0	mainstream mass flow rate
p	pressure
Pr	Prandtl number
R	gas constant
Re	Reynolds number
s	distance from the leading edge along the pressure ($s<0$) or suction surface ($s>0$) normalized by blade span at the trailing edge
T	temperature
Tu	turbulence intensity
v^*	shear velocity
V_c	average coolant velocity at the hole-exit
x,y,z	Cartesian coordinate system with z-coordinate along the span
y^+	distance in wall coordinates $(=yv^*/v)$
z_h	z for hub at trailing edge
z_n	$=(z-z_h)$/blade span at trailing edge
α	thermal diffusivity
Δy	distance (from the wall) of the first point off the wall
ε	turbulence dissipation rate
η	film-cooling effectiveness $[=(T_{o,rel}-T_{aw})/(T_{o,rel}-T_c)]$
μ	viscosity
ν	kinematic viscosity
ρ	density
ω	specific turbulence dissipation rate $(=\varepsilon/k)$
Ω	rotational speed of the blade

Subscripts

aw	corresponding to adiabatic condition
c	for coolant (average value)
ef	effective value
ex	value at exit
in	value at inlet
l	laminar value
o	stagnation value
rel	value relative to blade
T	turbulent value
w	value at wall

* Tel.: +1-216-433-6788; fax: +1-216-433-5802.
E-mail address: vijay.garg@grc.nasa.gov (V.K. Garg).

0142-727X/00/$ - see front matter
PII: S0142-727X(99)00072-7

1. Introduction

It is well known from the thermodynamic analysis that the performance of a gas turbine engine is strongly influenced by the temperature at the inlet to the turbine. There is thus a growing tendency to use higher turbine inlet temperatures, implying increasing heat loads to the engine components. Modern gas turbine engines are designed to operate at inlet temperatures of 1800–2000 K, which are far beyond the allowable metal temperatures. Thus, to maintain acceptable life and safety standards, the structural elements need to be protected against the severe thermal environment. This calls for an efficient cooling system. One such cooling technique currently

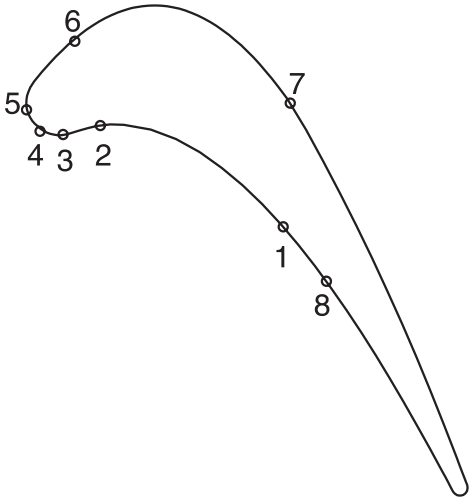

Fig. 1. Near mid-span profile of blade with hole-row locations.

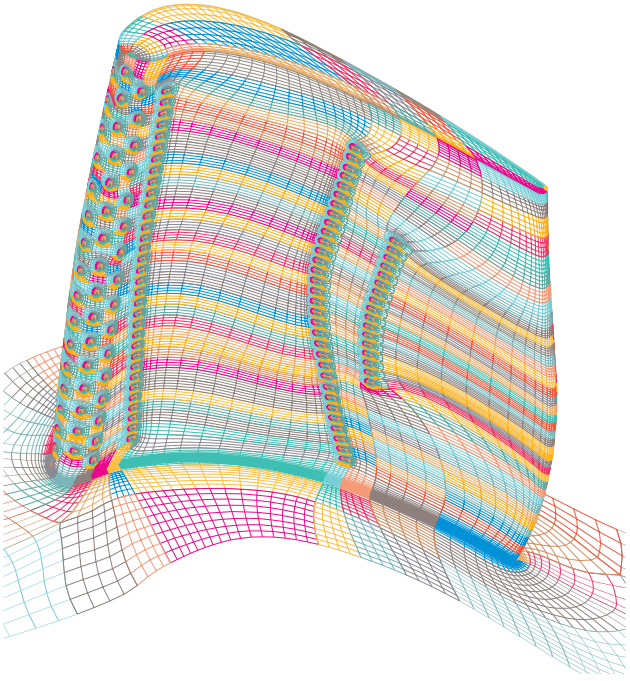

Fig. 2. Grid on the blade tip and pressure side, and a part of the hub (shows three staggered rows of shower-head holes and three rows of holes on the pressure side; two rows of holes on the suction side are not visible here).

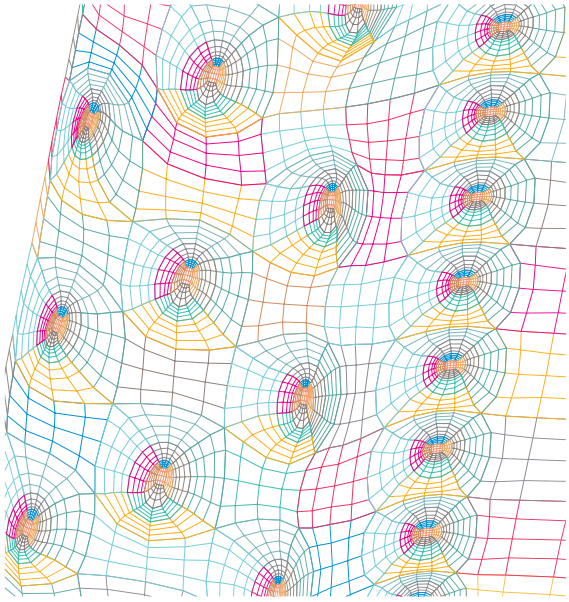

Fig. 3. Grid on the rotor (mid-span) surface near three staggered rows of shower-head holes and row #2 on the pressure surface.

Table 1
Parameter values[a]

Row #	Given m_c/m_o (%)	Computed m_c/m_o (%)	B_p
1	0.47	0.477	0.3393
2	0.51	0.508	0.357
3	0.65	0.419	0.19
4	0.65	0.145	0.19
5	0.65	0.086	0.19
6	0.49	0.493	0.4528
7	0.35	0.354	0.4756
8	0.21	0.214	0.2854

[a] $p_{o,in} = 329.36$ kPa; $T_{o,in} = 460$ K; $T_c = 221.1$ K; $p_{ex} = 101.35$ kPa; $\Omega = 11570.2$ rpm; $m_c/m_o = 0.0268$; $T_w = 297.2$ K or $\partial T/\partial n = 0$ at blade and hub.

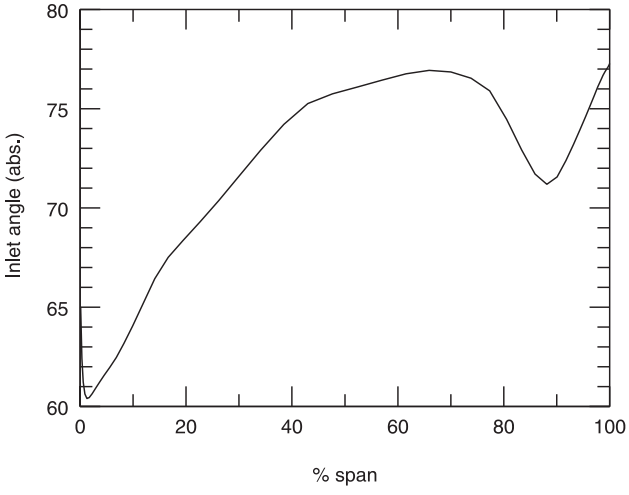

Fig. 4. Main flow angle at inlet to the rotor.

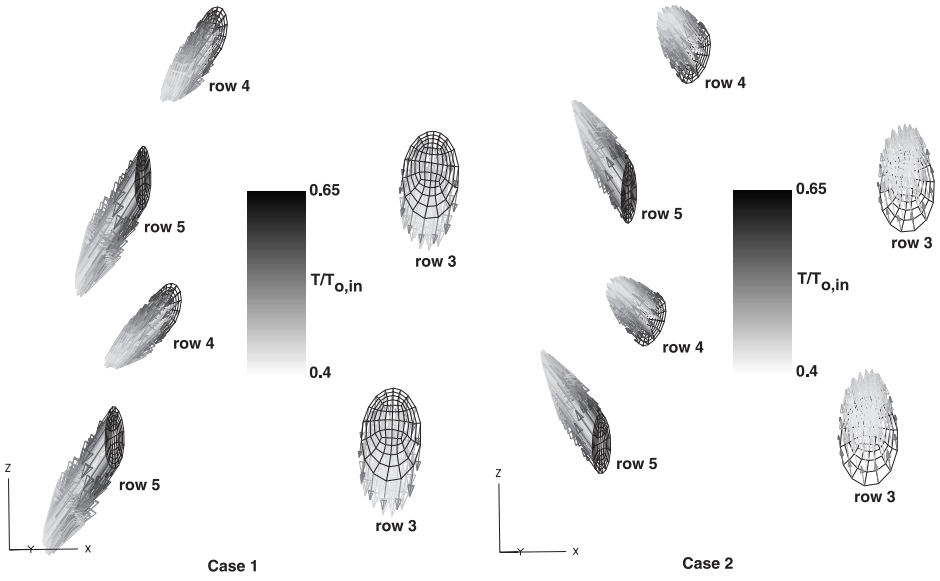

Fig. 5. Coolant velocity vectors, colored by temperature, at the exit of some shower-head holes near the hub.

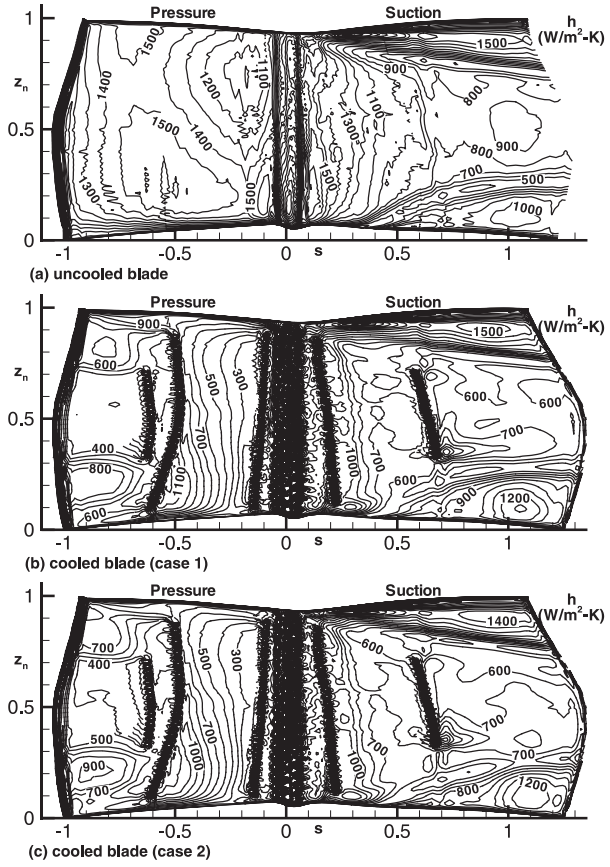

Fig. 6. Heat transfer coefficient on the blade surface using the tip model (no grid in the tip clearance gap).

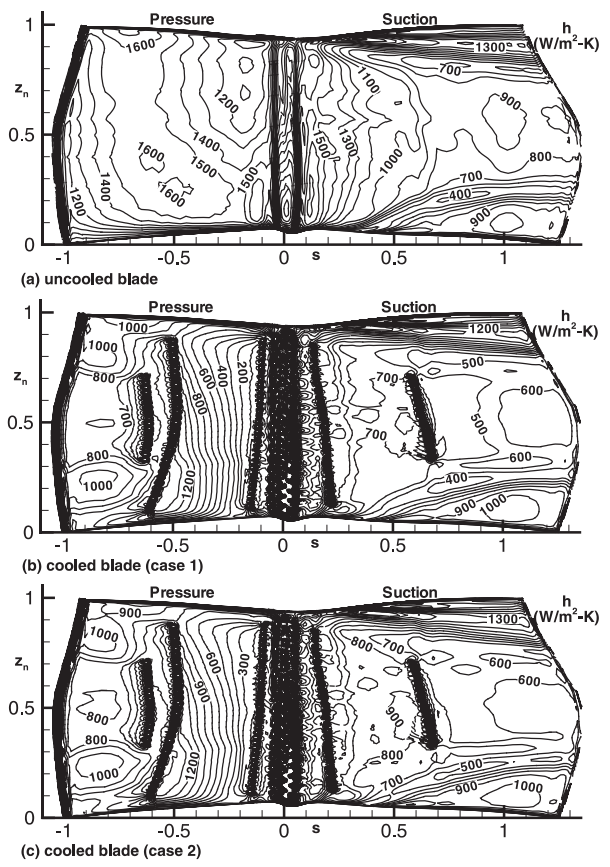

Fig. 7. Heat transfer coefficient on the blade surface (with grid in the tip clearance gap).

used for high temperature turbines is film cooling. In this technique, cooler air is injected into the high temperature boundary layer on the blade surface. Since the injected cooler air is bled directly from the compressor before it passes through the combustion chamber, it represents a loss in the total power output. The designer's goal is therefore to minimize the amount of coolant necessary to insure adequate engine life. Unfortunately, the thermal design of a film-cooled blade is still based on one-dimensional analysis and empirical correlations, thereby requiring actual testing

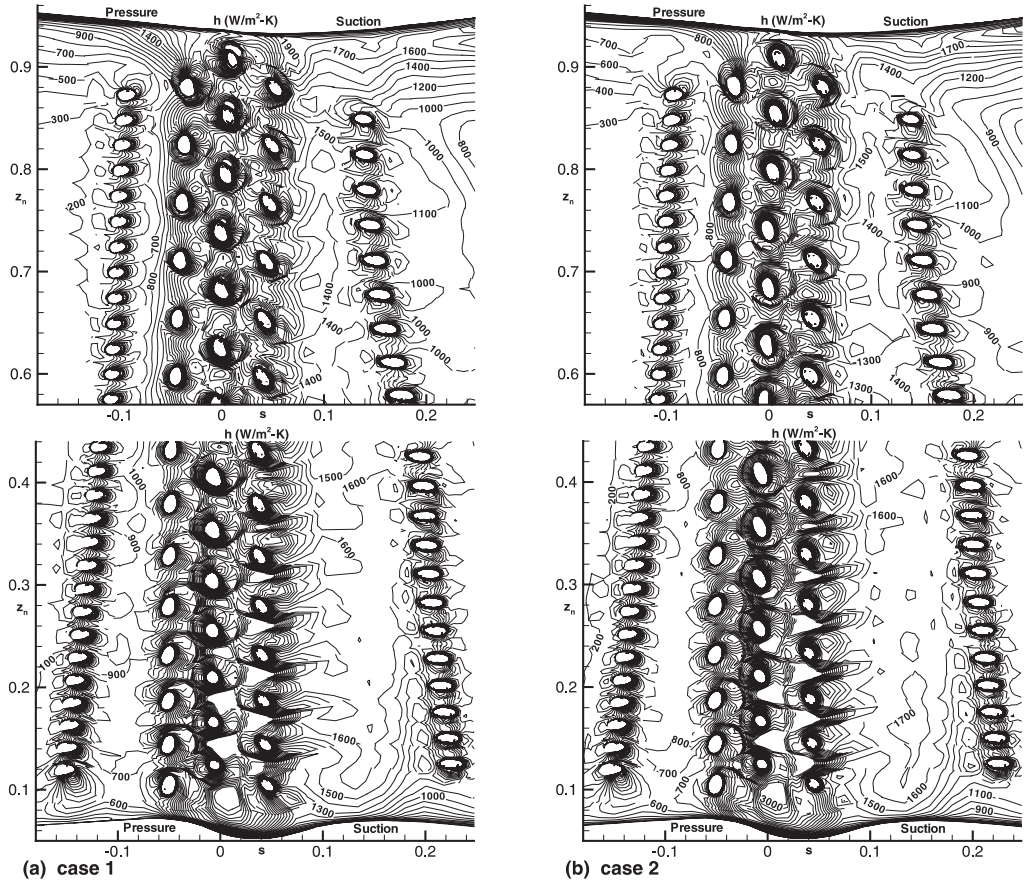

Fig. 8. Heat transfer coefficient in the leading edge region on the cooled blade surface (no grid on blade tip).

of every design concept. In such a situation, only minor variations of existing designs are adopted since any novel ideas are too expensive to test thoroughly. There is thus an urgent need to be able to predict accurately the heat transfer characteristics of film-cooled blades before actually testing them in the engine.

A considerable effort has been devoted to understanding the coolant film behavior and its interaction with the mainstream flow. The film-cooling performance is influenced by the wall curvature, three-dimensional external flow structure, free-stream turbulence, compressibility, flow unsteadiness, the hole size, shape and location, and the angle of injection. Interest in this field has grown considerably in recent years. However, many studies on film cooling have been confined to simple geometries, for example, two-dimensional flat and curved plates in steady, incompressible flow.

An excellent survey of the film-cooling work up to 1971 has been provided by Goldstein (1971). Several further studies in this field have been summarized by Garg and Gaugler (1993, 1994, 1996). A number of parametric studies have been performed by Garg and co-workers to determine the effect of several parameters, such as the effect of coolant velocity and temperature distributions at the hole-exit (Garg and Gaugler, 1997b), the effect of blade rotation and the direction of coolant ejection from the shower-head holes (Garg, 1997), the effect of spanwise pitch of shower-head holes (Garg and Gaugler, 1996), the effect of coolant to mainstream mass flow and temperature ratio (Garg and Gaugler, 1997a), and the effect of turbulence modeling (Garg and Abhari, 1997; Garg and Ameri, 1997; Garg, 1998, 1999a). Four turbulence models, the Baldwin–Lomax model, Coakley's q–ω model, Chien's k–ε model, and Wilcox's k–ω models have been analyzed, and results compared with the experimental data for heat transfer from rotating as well as stationary blades. In all these studies by Garg and co-workers, coolant velocity and temperature distributions were prescribed at the hole-exits. Moreover, while the true hole-exit on the blade surface is oval-shaped, it was approximated by a rectangle with steps owing to the use of a single-block grid. A recent study by Garg and Rigby (1999) analyzed in detail the coolant flow structure issuing out of compound-angled shower-head holes on a real blade. The flow was resolved not just over the blade but also inside the three staggered rows of film-cooling hole-pipes and in the plenum where the cooling flow originates. This study also presented an extensive survey of existing literature on the coolant flow characteristics at the exit of film-cooling holes.

We utilize the results of Garg and Rigby (1999) in studying the heat transfer characteristics of a three-dimensional high-pressure turbine rotor with 172 film-cooling holes in eight rows. We generate a multi-block grid that does not extend into the cooling hole pipes since there are too many (172) pipes. However, we retain the true shape of the hole-exits on the blade surface, and pack as many as 80 control volumes within each tiny hole-exit. Then we prescribe polynomial velocity and temperature distributions for the coolant flow at these hole-exits. For the rotating case, the complete blade, the hub and the shroud with a tip clearance region are analyzed. Results for the heat transfer coefficient on the blade, hub and shroud corresponding to an isothermal condition, and for the film-cooling effectiveness on an adiabatic blade are presented.

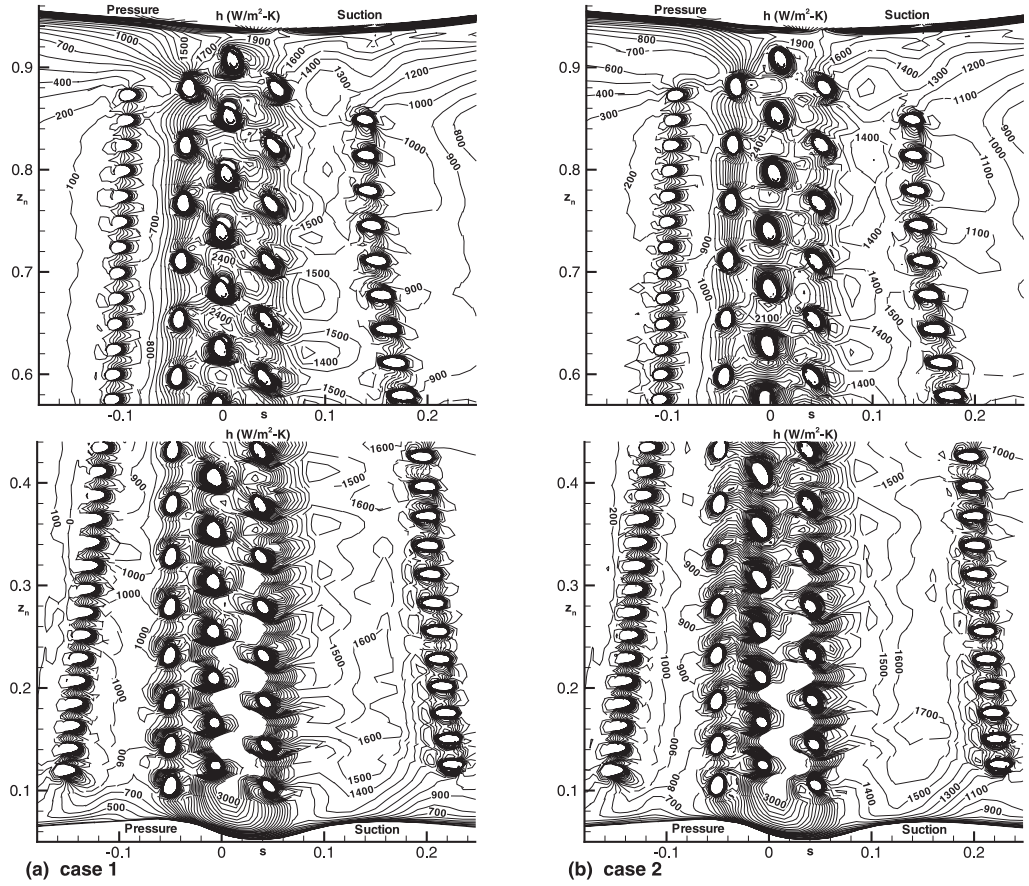

Fig. 9. Heat transfer coefficient in the leading edge region on the cooled blade surface (with grid on blade tip).

2. Analysis

The numerical simulation has been performed using the NASA Glenn Research Center General Multi-Block Navier–Stokes Convective Heat Transfer code, Glenn-HT. Briefly, the code, formerly known as TRAF3D.MB (Steinthorsson et al., 1993, 1997), is an explicit, multigrid, cell-centered, finite volume code with a k–ω turbulence model without any wall functions. This is a general purpose flow solver designed for simulations of flows in complicated geometries. The Navier–Stokes equations in a rotating Cartesian coordinate system are mapped onto a general body-fitted coordinate system using standard techniques. The multistage Runge–Kutta scheme developed by Jameson et al. (1981) is used to advance the flow solution in time from an initial approximation to the steady state. A spatially varying time step along with a CFL number of 4 is used to speed convergence to the steady state. Eigenvalue-scaled artificial dissipation and variable-coefficient implicit residual smoothing are used along with a full-multigrid method. The overall accuracy of the code is second-order. A single-block version of the same code, modified for film-cooling applications, was used by Garg and co-workers for the film-cooling studies described earlier, except for the study by Garg and Rigby (1999) which utilized the multi-block code. The k–ω model of Wilcox (1994) with Menter's modifications (Menter, 1993) has yielded good results for heat transfer on film-cooled blades (Garg and Ameri, 1997; Garg, 1999a), and is highly desirable for multi-block codes since it does not require the computation of distance from a wall. Also, no wall functions are used; thus the grid extends to the wall with $y^+ < 1$ for the first grid point off the wall. This eliminates any bias to the complex interactions between the coolant and the mainstream near the blade surface.

It is assumed that the effective viscosity for turbulent flows can be written as

$$\mu_{\mathrm{ef}} = \mu_{\mathrm{l}} + \mu_{\mathrm{T}},$$

where the laminar viscosity μ_{l} is calculated using a power-law for its dependence on temperature. The turbulent viscosity μ_{T} is computed using the low-Re k–ω model described by Garg and Ameri (1997) and Ameri et al. (1997). The turbulent thermal diffusivity is computed from

$$\alpha_{\mathrm{T}} = \frac{\mu_{\mathrm{T}}}{\rho Pr_{\mathrm{T}}},$$

where a constant value of 0.9 is used for the turbulent Prandtl number, Pr_{T}.

3. Boundary conditions

At the main flow inlet boundary located at an axial distance approximately equal to the blade axial chord at mid-span upstream of the blade leading edge, the total temperature, total pressure, and flow angle are specified, and the upstream-running Riemann invariant based on the total absolute velocity is calculated at the first interior point and extrapolated to the inlet. The velocity components are then decoupled algebraically, and the density is found from total temperature, total pressure and total velocity using an isentropic relation. For the turbulence model, the value of k and ω is specified using the experimental conditions, namely

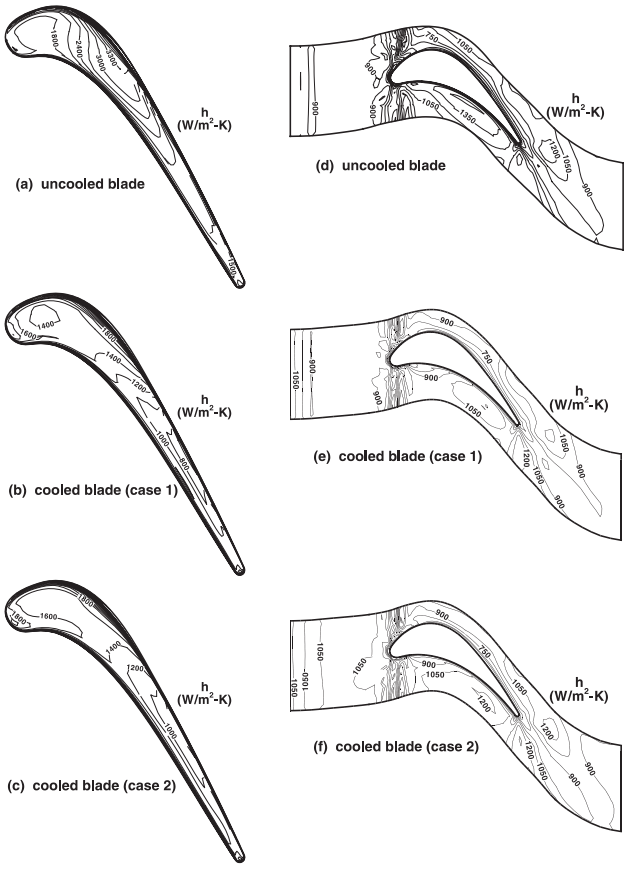

Fig. 10. Heat transfer coefficient on the blade tip and the hub (with grid on blade tip).

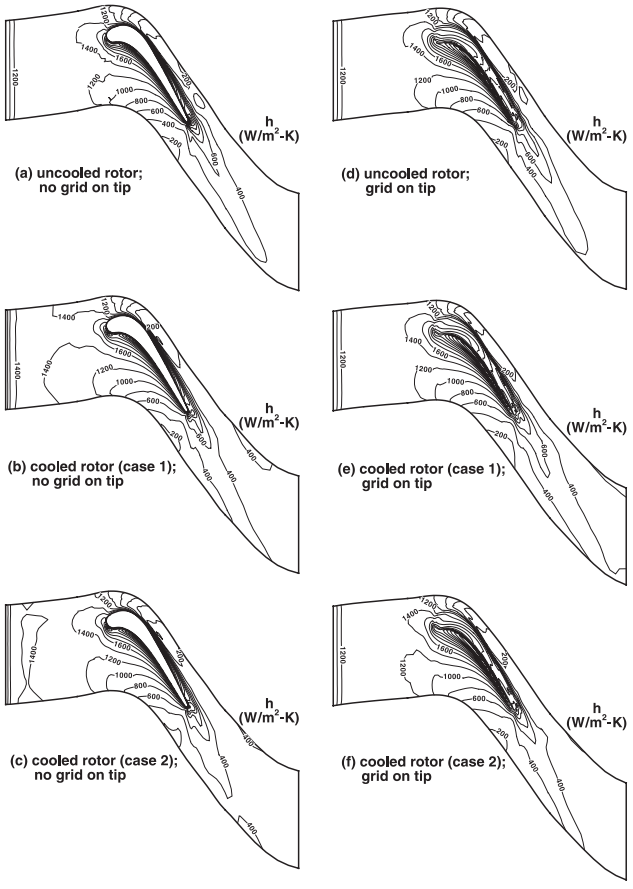

Fig. 11. Heat transfer coefficient on the shroud for various cases.

$$k = 1.5(u_{\text{in}} Tu_{\text{in}})^2, \quad \omega = k^{1/2}/l,$$

where Tu_{in} is the intensity of turbulence at the inlet (taken to be 0.05), u_{in} the inlet velocity, and l the turbulence length scale representing the size of the energy containing eddies. This length scale is usually not reported as part of the experimental conditions, and needs to be assumed. For the present study, l was assumed to be 4% of the blade axial chord at mid-span. It may be noted that Garg and Ameri (1997) found negligible difference in the heat transfer coefficient at the surface of a film-cooled blade under similar mainstream conditions when Tu_{in} was raised to 0.15, and l was taken to be 0.01 or 0.25 at the inlet, using the k–ε model. It is expected that a similar conclusion holds for the k–ω model for the present blade as well.

At the main flow exit plane located at an axial distance approximately equal to the blade axial chord at mid-span downstream of the blade trailing edge, the static pressure is specified and the density and velocity components are extrapolated from the interior. The local static pressure is found by integrating the axisymmetric radial equilibrium equation. At the solid surfaces of the rotating blade, hub and shroud, the no-slip condition is enforced, and either the isothermal $(T_{\text{w}}/T_{\text{o,in}} = 0.646)$ or adiabatic condition is specified. The boundary conditions for turbulence quantities on the walls are $k = 0$, and

$$\omega = 100 \left.\frac{\partial u}{\partial y}\right|_{\text{wall}}$$

for a hydraulically smooth surface. An upper limit is imposed on the value of ω at the wall, as suggested by Menter (1993) and found effective by Chima (1996),

$$(\omega_{\max})_{\text{wall}} = \frac{800}{Re} \frac{v}{(\Delta y)^2}.$$

The grid around the blade extends to mid-way between two adjacent blades with periodic flow conditions in terms of cylindrical velocity components set on a dummy grid line outside this boundary. The boundary layer thickness on the hub and shroud was taken to be 7% of the blade span for the incoming flow to the rotor. The tip clearance region was handled either by imposing periodicity conditions across the airfoil thus requiring no grid in the tip clearance gap or by gridding the gap whereby no periodicity condition need be used. The effect of both these approaches will be described.

The effects of film cooling have been incorporated in the form of appropriate boundary conditions at the hole locations on the blade surface. Each hole-exit in its true oval shape is represented by 80 control volumes. Different velocity and temperature profiles for the injected coolant can be specified at the hole-exits. For the present results, polynomial distribution (Garg and Gaugler, 1997b) of coolant velocity (relative to the blade) and temperature at the hole-exit was specified. Turbulent intensity at the hole-exit was assumed to be 0.1, while the turbulence length scale at the hole-exit was taken to be $0.25d$. It has been reported by Garg (1999a), however, that changing Tu to half the value and/or l by a factor of 5 at the hole-exit resulted in a negligible change in heat transfer coefficient at the surface of ACE rotor, except in the immediate vicinity of the holes. It is expected that a similar result would hold for the present rotor.

4. Blade details

The turbine blade profile near mid-span along with the cooling row locations is shown in Fig. 1. There are 38 blades in the rotor. The number of holes in rows 1 through 8 are 32, 33, 16, 16, 16, 25, 17 and 17, respectively. The holes are all cylindrical with a diameter of 0.381 mm. Three rows (#3, 4, 5) are staggered with compound-angled holes on the showerhead. For these three rows, the hole angle with the spanwise direction varies approximately from 24° to 66°, and with the streamwise direction from 85° to 123°. For other rows of holes, the hole angle is 90° with the spanwise direction and varies from 24° to 45° with the streamwise direction.

5. Computational details

The flow domain consists of the entire, three-dimensional, rotating blade with 172 film-cooling holes in eight rows including three staggered rows of compound-angled showerhead holes, the hub, the shroud and the tip clearance region. The fact that the hole diameter is only 0.381 mm, about 1% of the blade axial chord at mid-span, and the tip clearance region is only about 1.3% of the blade span presents a challenge for grid generation. A multi-block grid is generated for the complex geometry using the commercial code GridPro/az3000 (Program Development Corporation, 1997). This consists of generating a system of locally structured grid blocks in a globally unstructured assembly. The grid generation code produces a body-fitted multi-block grid with hexahedral cells and full face-matching blocks.

Some details of the viscous grid are shown in Fig. 2. In this figure and in Fig. 3, each elementary block is shown in a different shade of gray. The inviscid grid is first generated and the viscous grid is then obtained from the inviscid grid by clustering the grid near all the solid walls. The clustering is done in such a way as to ensure that in the viscous grid, the distance of the first grid point off a solid wall, measured in wall units (y^+), is less than unity for the cases studied here, following Boyle and Giel (1992). Moreover, the clustered viscous grid near all wall boundaries does not extend into the far-flow field. A blow-up of the grid near the shower-head hole-exits as well as one row (#2) on the pressure surface is shown in Fig. 3. It may be noted that the exact oval shape of the hole opening on the blade surface is faithfully discretized. Also, the multi-block grid is able to transition smoothly from a very fine structure near locations of complex geometry such as hole boundaries to a coarse structure away from the holes. As can be observed from these figures, the grid quality is very good.

Initially, the grid consists of 4818 or 4784 elementary blocks depending upon whether the tip clearance gap is gridded or not, but before the solver is used, it can be merged into 280 or 276 super blocks using the Method of Weakest Descent (Rigby, 1996; Rigby et al., 1997). For so many super blocks, generation of the connectivity file and the data file for the application of boundary conditions was automated. For the 280 super blocks, there were a total of 1016 boundary condition patches on the blade surface, of which 516 were over the 172 hole-exits and the remaining 500 on the blade solid surface including the tip. An additional 15 boundary condition patches covered the hub, the shroud, and inlet and exit for the main flow. In the above details, periodic boundary condition patches are not accounted for since the code takes care of periodicity via the connectivity data for the blocks.

The final viscous grid in 280 super blocks consists of a total of 1,987,520 cells, with 80 cells in each of the 172 hole-exits. For computational accuracy the ratio of two adjacent grid sizes in any direction was kept within 0.8–1.25. We may point out that using the commercial code GridPro/az3000, two multi-block grids were first generated for the uncooled rotor for a grid independence study. One grid had twice as many cells in the streamwise direction as the other grid. The two grids yielded nearly identical heat transfer coefficient and pressure distributions at the blade surface. Computations were run in multi-processor mode on the 16-processor C90 or J90 supercomputer at NASA Ames Research Center. The code requires about 275 Mw of core storage with all blocks in the core memory, and another 40 Mw of scratch disk space. It takes about 90 s per iteration at the finest grid level. A case requires about 1500 iterations to converge.

6. Results and discussion

Results are presented for the heat transfer coefficient at the blade including the tip, hub and shroud surfaces for isothermal walls, and also for film-cooling effectiveness on an adiabatic blade. Values for the various parameters for which the present simulation is performed are listed in Table 1, and the inlet angle for the main flow is shown in Fig. 4. Values of the blowing parameter were adjusted so that the computed and given coolant mass flow ratios match, as is evident from Table 1. B_p varied from row to row except that it was the same for

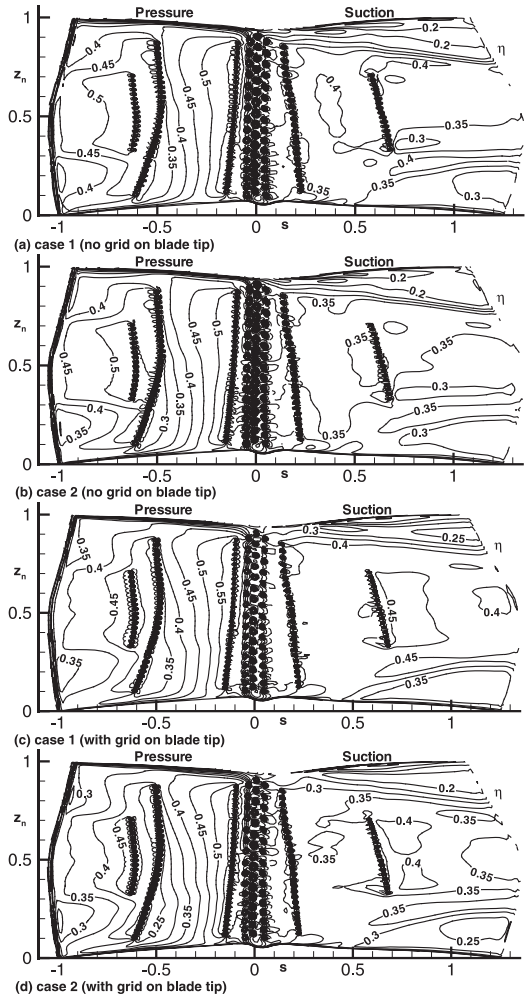

Fig. 12. Film-cooling effectiveness on the adiabatic blade surface.

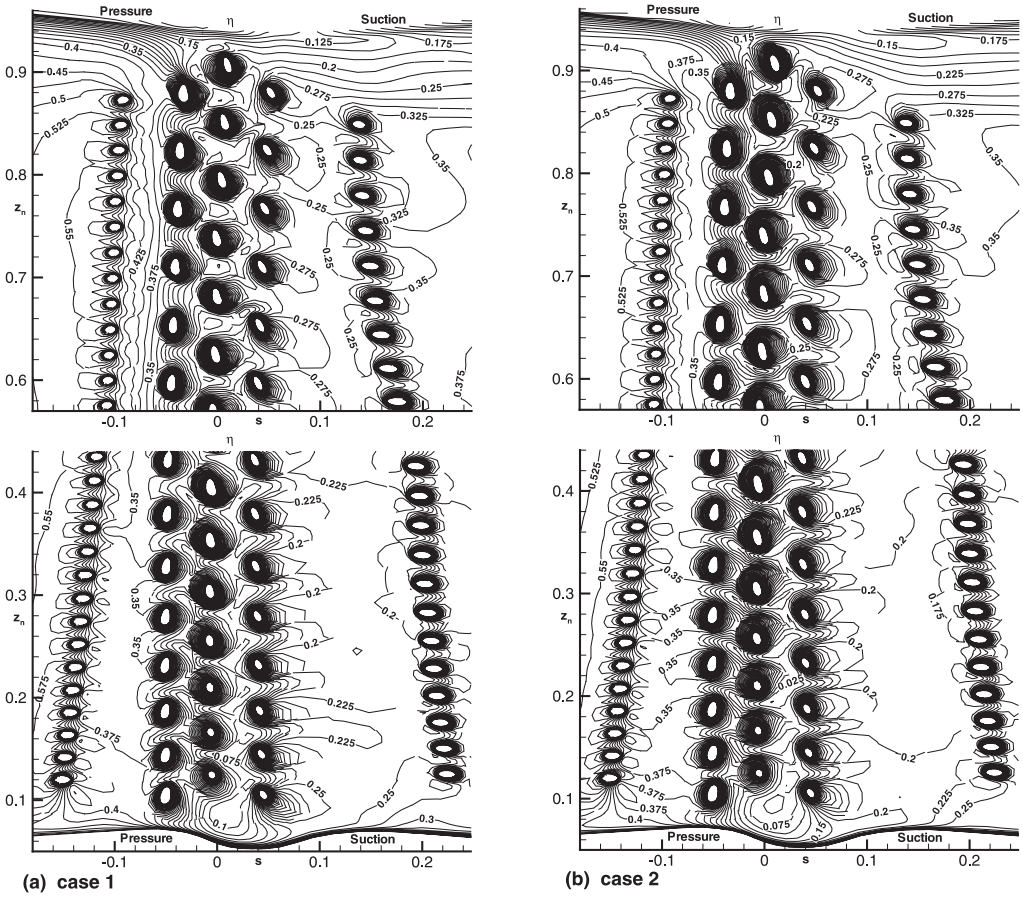

Fig. 13. Film-cooling effectiveness in the leading edge region on the adiabatic blade surface (no grid on blade tip).

the shower-head rows 3, 4 and 5; also it was kept the same for all holes in a row. For the shower-head rows 3, 4 and 5, the total coolant mass flow rate was given. While the computed total coolant mass flow for these rows is the same, it is instructive to look at the distribution which is like 4.8:1.7:1.0 through rows 3, 4 and 5. This is due to the static pressure distribution around the leading edge. It may be noted that the stagnation line for the main flow is either between rows 4 and 5 or between rows 3 and 4, as shown later (Fig. 17). For the cooled isothermal or adiabatic blade, two orientations of the shower-head hole rows 3, 4 and 5 were analyzed; one called 'case 1' refers to coolant ejection from the shower-head holes towards the hub, and another called 'case 2' refers to this ejection towards the blade tip, as exemplified in Fig. 5 by the coolant velocity vectors, colored by temperature, at the exit of a few shower-head holes near the hub.

Fig. 6 compares the heat transfer coefficient on the uncooled blade surface with that on the cooled blade surface for both orientations of the shower-head holes when there is no grid in the tip clearance gap. These distributions are represented on the s–z_n plane, where s is the surface distance along the pressure or suction surface measured from the leading edge, and z_n is the z-coordinate measured from that for hub at the blade trailing edge, both normalized by the span at the trailing edge of the blade. We note that the heat transfer coefficient is high in the leading edge region between the hub and blade mid-span, and all along the tip of the blade (even on the cooled blade); it is also high on the suction surface near the tip just downstream of the leading edge. This is due to the flow crossing over from the pressure to the suction side through the tip clearance gap. High values of h in the leading edge region of the cooled blade are due to rather low amount of coolant injected through the shower-head rows of holes. In fact, the portion of the blade leading edge between the hub and blade mid-span is not covered by the coolant at all, as is evident from the streamlines shown in Fig. 17. The heat transfer coefficient on the cooled blade surface is generally lower, specially on the pressure surface, than that on the uncooled blade. While h varies considerably in both the streamwise and spanwise directions on the suction surface, its spanwise variation is weaker than the streamwise variation on the pressure surface except in the boundary layers near the hub and tip. For the uncooled blade, the heat transfer coefficient is almost uniform over a large part of the pressure surface. For the cooled blade, there is little difference between the h distributions for the two orientations of shower-head holes.

Fig. 7 shows the heat transfer coefficient on the uncooled and cooled blade surface when there is a grid in the tip clearance gap. Results in Fig. 7 are very similar to those in Fig. 6, with one exception. The blade tip region on the suction side has much lower heat transfer coefficient for all cases in Fig. 7 as compared to those in Fig. 6. This is due to the fact that periodicity across the tip clearance gap, while using the tip model, ensures the same flow characteristics on both the pressure and suction sides of the tip. Without the tip model, the flow is allowed to develop through the tip clearance gap. Except for this difference in a narrow region, the tip clearance model used for the results in Fig. 6, with no grid in the tip clearance gap, seems to work fairly well as far as heat transfer coefficient on the blade surface is concerned.

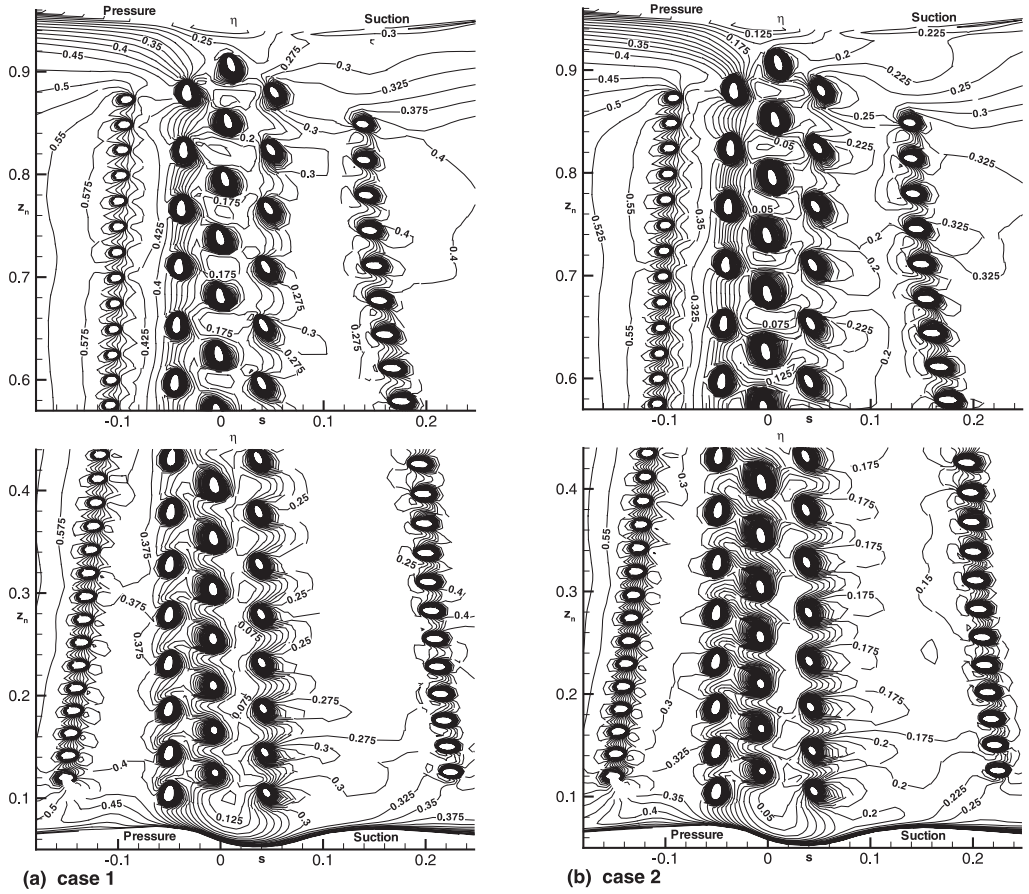

Fig. 14. Film-cooling effectiveness in the leading edge region on the adiabatic blade surface (with grid on blade tip).

Figs. 8 and 9 provide a close-up view of the h values in the leading edge region of the cooled blade for both orientations of shower-head holes without and with the grid in the tip clearance gap. For each case, rows #2 and 6 on the pressure and suction side are also shown along with the three staggered rows on the shower-head. The region between rows 4 and 5 on the suction side has high heat transfer coefficient, specially between the hub and blade mid-span. This is due to the fact that the stagnation line for the main flow falls between rows four and five over this region of the blade. Thus this portion of the leading edge is not covered by the coolant at all (cf. Fig. 17). Also, the blade tip on the pressure side (cf. Fig. 9) has high heat transfer coefficient. This may not be true for the real blade since the film-cooling holes in the blade tip were not included in the present study. While differences between the four cases shown in Figs. 8 and 9 are small, it does appear that coolant ejection (from shower-head holes) towards the blade tip (case 2) leads to somewhat lower values of h in the upper half of the leading edge region.

Fig. 10 compares the heat transfer coefficient on the blade tip and hub for the uncooled and cooled blade cases with a grid in the tip clearance gap. Of course, with no grid in the tip clearance gap, it is not possible to compute the heat transfer coefficient on the blade tip. Values of h are much higher on the uncooled blade tip as compared to those on the cooled blade tip. In both cases, however, the suction side of the blade tip, just downstream of the thickest blade section, experiences the highest heat transfer coefficient. This is due to the high flow velocity caused by the mainstream flow crossing from the pressure to the suction side of the blade through the tip clearance gap, as shown later in Figs. 15 and 16. For the heat transfer coefficient on the hub, differences between the uncooled and cooled blade cases are small, except on the pressure side of the blade. For the cooled blade, some of the coolant from holes on the blade near the hub flows over to the hub (cf. Fig. 17) causing a reduction in the heat transfer coefficient. The h values for the cooled blade case 1 (Fig. 10(e)) are generally lower than those for case 2 (Fig. 10(f)), as expected, since for the former, the shower-head holes inject the coolant towards the hub. It may also be noted that h values on the hub are much smaller than those on the blade surface (Figs. 6–9), blade tip (Fig. 10) and the shroud (Fig. 11). The high values of h on the hub near the blade leading edge are due to a kink in the hub surface caused by the blade outline at the hub.

Fig. 11 displays the heat transfer coefficient on the shroud for the uncooled and cooled blade cases with and without a grid in the tip clearance gap. While the results for the six cases shown in Fig. 11 are quite similar, major differences arise whether the tip clearance gap is gridded. Without a grid in the tip clearance gap, a part of the shroud directly above the blade tip has no means to compute any flow characteristics, representing an unrealistic situation. With the tip clearance gap gridded, we do find high values of h in the region of the shroud directly above the blade tip, due to the mainstream flow crossing from the pressure to the suction side through the gap, thereby impinging on the shroud.

Fig. 12 shows the film-cooling effectiveness distribution on the adiabatic blade surface represented by s–z_n coordinates for both orientations of the shower-head holes with and without a grid in the tip clearance gap. The effectiveness is the lowest in

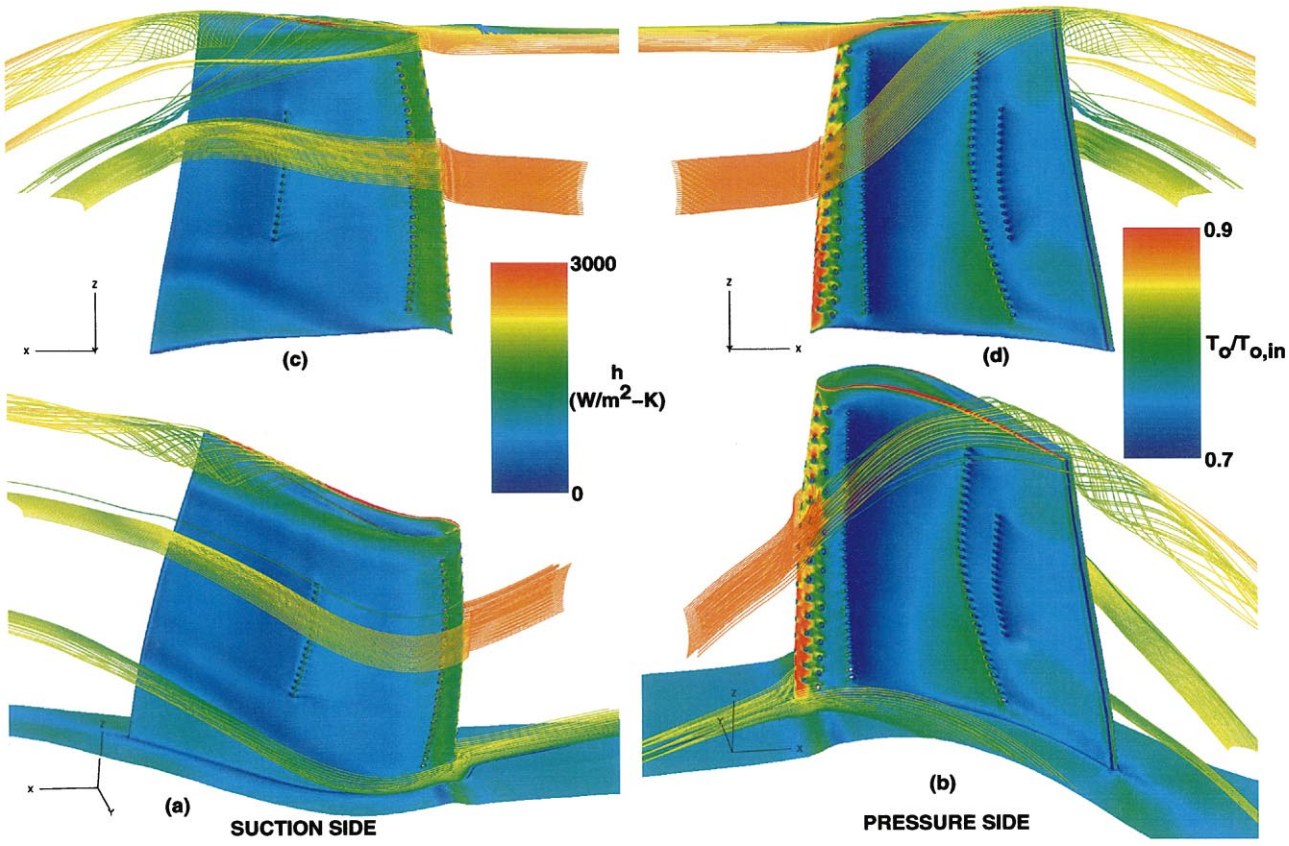

Fig. 15. Streamlines, colored by temperature, over the cooled blade surface with distribution of h (case 1; grid on blade tip).

the leading edge region and near the tip, specially over the suction surface. Since h and η are both based on the difference from $T_{o,rel}$, it is natural to expect low values of η where h is high, and vice versa (cf. Figs. 6 and 7). Figs. 13 and 14 show the details of film-cooling effectiveness in the leading edge region near rows 2–6 for both orientations of the shower-head holes with and without a grid in the tip clearance gap. The low effectiveness regions over the blade leading edge are clearly highlighted.

Fig. 15 shows the streamlines, colored by stagnation temperature, approaching the cooled blade near the hub, mid-span and tip for case 1 with grid on the blade tip. The hub is also shown in Fig. 15(a) and (b). The heat transfer coefficient distribution is shown on the blade surface and the hub in this figure and in Figs. 16 and 17. In Fig. 15(a) and (b), there is some evidence of the horse-shoe vortex near the hub. Also, the mainstream approaching the blade mid-span splits at the leading edge such that the part on the pressure side heads towards the blade tip, crossing over through the tip clearance gap and producing a complex vortical structure on the suction side of the blade near the tip. Fig. 15(c) and (d) show that the flow approaching the tip also splits at the leading edge but the part on the pressure side immediately crosses over to the suction side through the tip clearance gap, and ends up (in green color) in a complex vortical structure on the suction side close to the mid-span; the part on the suction side (in yellow color) stays between the mid-span and tip. Comparing Fig. 15(a) and (c), it is evident that the entire flow that approached the blade near the tip ends up (on the suction side) below the flow that approached the blade at mid-span initially.

Fig. 16 shows the streamlines, colored by stagnation temperature, approaching the cooled blade near the hub and several sections of the span for case 1 with grid on the blade tip. Fig. 16(a) shows the passage vortex flow clearly on the suction side of the blade while Fig. 16(b) shows more evidence of the horse-shoe vortex. Fig. 16(d) shows that the mainstream approaching the blade between the hub and mid-span splits at the leading edge such that the part over the pressure surface covers almost the entire pressure side from hub to tip. Also, a part of the mainstream between mid-span and blade tip crosses over to the suction side through the tip clearance gap while the rest remains on the pressure side, unmixed with the coolant (orange color). Comparison of Figs. 15(a) and 16(c) reveals the contribution of various streams along the blade span to the vortical structures on the suction side of the blade.

Fig. 17 shows the streamlines, colored by stagnation temperature, emanating from holes over the cooled blade surface for case 1 with grid on the blade tip. While the complex vortical structure is clearly visible on the suction side near the blade tip (Fig. 17(a)), more interesting is the split of coolant flow from the leading edge hole row #4 in Fig. 17(b). A close look at Fig. 17(b) reveals that the coolant from the lower eight holes in row #4 flows towards the pressure side, while that from the upper eight holes flows towards the suction side. Thus, the stagnation line for the mainstream flow is between rows 4 and 5 from hub to blade mid-span, and between rows 3 and 4 from mid-span to blade tip. Due to this, there is no coolant over the leading edge region of the blade from hub to mid-span between rows 4 and 5. This leads to the high heat transfer coefficient or the low effectiveness values in this part of the blade. Also clear from Fig. 17(b) is that some of the coolant from holes near the hub in rows 2 and 3 flows towards the hub. This leads to a reduction in the heat transfer

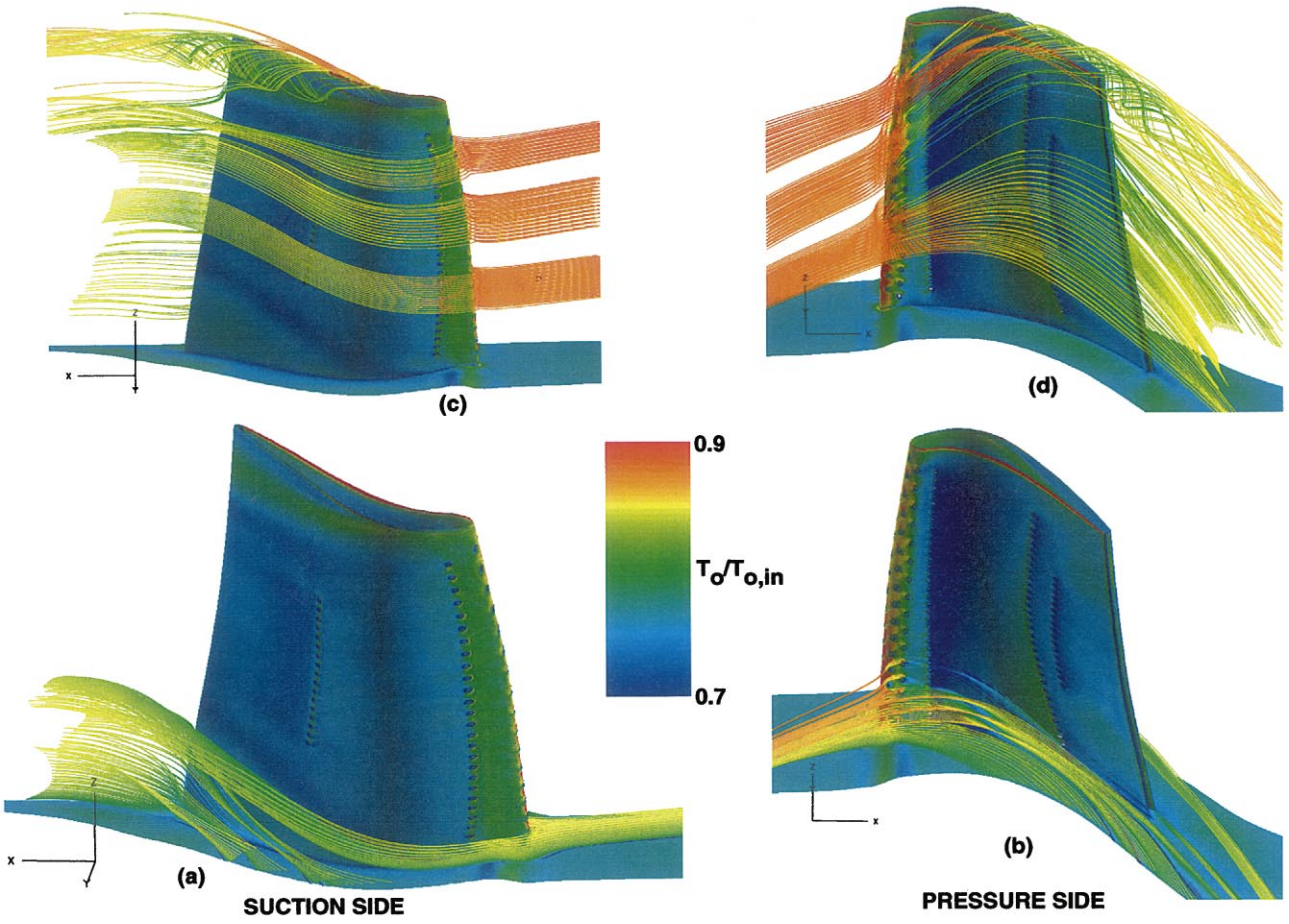

Fig. 16. Streamlines, colored by temperature, over the cooled blade surface with distribution of h (case 1; grid on blade tip).

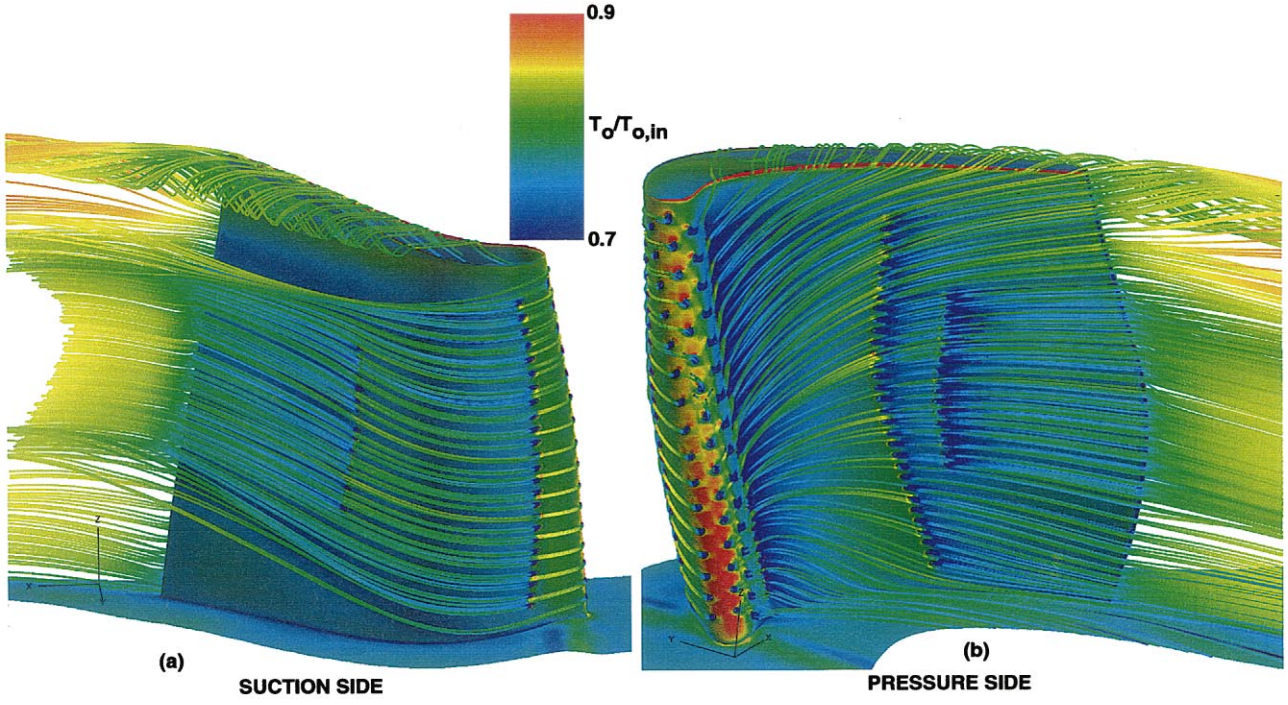

Fig. 17. Streamlines, colored by temperature, emanating from holes over the cooled blade surface with distribution of h (case 1; grid on blade tip).

coefficient on the part of hub near the pressure side of the cooled blade (cf. Fig. 10(d) and (e)).

For the sake of brevity, pressure and y^+ (for the first cell off a solid surface) distributions are not presented here. They are available in Garg (1999b) for case 1 with no grid in the tip clearance gap. We may note, however, that pressure distribution is little affected by film cooling, as is well known. Also, y^+ values were found to be less than unity for all solid surfaces (blade, hub and shroud), in conformity with the requirement laid down by Boyle and Giel (1992) for accurate heat transfer prediction.

7. Conclusions

A multi-block, three-dimensional Navier–Stokes code has been used to compute heat transfer coefficient on the blade, hub and shroud for a rotating high-pressure turbine blade with 172 film-cooling holes in eight rows. Film-cooling effectiveness is also computed on the adiabatic blade. Wilcox's k–ω model is used for modeling the turbulence. It is found that for the given parameters, heat transfer coefficient on the cooled, isothermal blade is highest in the tip region, and in the leading edge region between the hub and blade mid-span. Also, the effectiveness over the cooled, adiabatic blade is the lowest in these regions. In the leading edge region between the hub and blade mid-span, high values of h and low values of η are due to the absence of coolant over this portion of the blade, caused by the stagnation line falling between the hole rows 4 and 5. In the tip region, they are due to the mainstream flow crossing over from the pressure to the suction side through the tip clearance gap. Results for an uncooled blade are also shown, providing a direct comparison with those for the cooled blade. Also, the heat transfer coefficient is much higher on the blade tip and shroud as compared to that on the hub for both the cooled and the uncooled cases, again due to the flow through the tip clearance gap. The effect of gridding the tip clearance gap vs. use of a tip clearance model is found to be small as far as the heat transfer coefficient or the adiabatic film-cooling effectiveness on the blade surface is concerned. However, for heat transfer from the blade tip and the shroud, the tip clearance gap must be gridded. Use of a tip clearance model not only yields unrealistic values of heat transfer coefficient on the shroud, it cannot provide these values on the blade tip at all. The effect of different orientation of coolant ejection from shower-head holes is found to be small for heat transfer from the blade (including the tip), hub and shroud.

Acknowledgements

The author wishes to thank Dr. Raymond Gaugler, Chief, Turbine Branch, Mr. John Rohde of the Subsonic Systems Office, and Mr. K.C. Civinskas, Turbine and Combustor Technology Program Manager at the NASA Glenn Research Center, and Mr. Milt Ortiz of AlliedSignal Engines for their support of this work. Geometric and other details for the blade obtained from Dr. Yong Kim and Dr. Jong Liu of AlliedSignal Engines are also acknowledged.

References

Ameri, A.A., Steinthorsson, E., Rigby, D.L., 1997. Effect of squealer tip on rotor heat transfer and efficiency, ASME Paper 97-GT-128.

Boyle, R.J., Giel, P., 1992. Three-dimensional Navier–Stokes heat transfer predictions for turbine blade rows, AIAA Paper 92-3068.

Chima, R.V., 1996. A k-ω turbulence model for quasi-three-dimensional turbomachinery flows, AIAA Paper 96-0248.

Garg, V.K., 1997. Adiabatic effectiveness and heat transfer coefficient on a film-cooled rotating blade. Numer. Heat Transfer, Part A 32, 811–830.

Garg, V.K., 1998. Heat transfer on a film-cooled rotating blade using a two-equation turbulence model. Int. J. Rotating Machinery 4 (3), 201–216.

Garg, V.K., 1999a. Heat transfer on a film-cooled rotating blade using different turbulence models. Int. J. Heat Mass Transfer 42 (5), 789–802.

Garg, V.K., 1999b, Heat transfer on a film-cooled rotating blade, ASME Paper 99-GT-44.

Garg, V.K., Abhari, R.S., 1997. Comparison of predicted and experimental Nusselt number for a film-cooled rotating blade. Int. J. Heat & Fluid Flow 18, 452–460.

Garg, V.K., Ameri, A.A., 1997. Comparison of two-equation turbulence models for prediction of heat transfer on film-cooled turbine blades. Numer. Heat Transfer, Part A 32, 347–371.

Garg, V.K., Gaugler, R.E., 1993. Heat transfer in film-cooled turbine blades, ASME Paper 93-GT-81.

Garg, V.K., Gaugler, R.E., 1994. Prediction of film cooling on gas turbine airfoils, ASME Paper 94-GT-16.

Garg, V.K., Gaugler, R.E., 1996. Leading edge film cooling effects on turbine blade heat transfer. Numer. Heat Transfer, Part A 30, 165–187.

Garg, V.K., Gaugler, R.E., 1997a. Effect of coolant temperature and mass flow on film cooling of turbine blades. Int. J. Heat Mass Transfer 40, 435–445.

Garg, V.K., Gaugler, R.E., 1997b. Effect of velocity and temperature distribution at the hole exit on film cooling of turbine blades. J. Turbomachinery 119, 343–351.

Garg, V.K., Rigby, D.L., 1999. Heat transfer on a film-cooled blade-effect of hole physics. Int. J. Heat & Fluid Flow 20, 10–25.

Goldstein, R.J., 1971. Film Cooling, Advances in Heat Transfer, vol. 7, Academic Press, New York, pp. 321–379.

Jameson, A., Schmidt, W., Turkel, E., 1981. Numerical solutions of the Euler equations by finite volume methods using Runge–Kutta time-stepping schemes, AIAA Paper 81-1259.

Menter, F.R., 1993. Zonal two-equation k–ω turbulence models for aerodynamic flows, AIAA Paper 93-2906.

Program Development Corporation, 1997. GridPro™/az3000 – User's Guide and Reference Manual, White Plains, NY.

Rigby, D.L., 1996. Method of weakest descent for automatic block merging, in: Proceedings of the 15th International Conference on Numerical Methods in Fluid Dynamics, Monterey, CA.

Rigby, D.L., Steinthorsson, E., Coirier, W.J., 1997. Automatic block merging using the method of weakest descent, AIAA Paper 97-0197.

Steinthorsson, E., Ameri, A.A., Rigby, D.L., 1997. TRAF3D.MB-A multi-block flow solver for turbomachinery flows, AIAA Paper 97-0996.

Steinthorsson, E., Liou, M.S., Povinelli, L.A., 1993. Development of an explicit multiblock/multigrid flow solver for viscous flows in complex geometries, AIAA Paper 93-2380.

Wilcox, D.C., 1994. Simulation of transition with a two-equation turbulence model. AIAA J. 32, 247–255.